

Aerosol Science and Technology

ISSN: 0278-6826 (Print) 1521-7388 (Online) Journal homepage: www.tandfonline.com/journals/uast20

Drag on Nonspherical Objects

David Leith

To cite this article: David Leith (1987) Drag on Nonspherical Objects, Aerosol Science and Technology, 6:2, 153-161, DOI: 10.1080/02786828708959128

To link to this article: https://doi.org/10.1080/02786828708959128

Published online: 06 Jun 2007.

Submit your article to this journal

Article views: 15064

View related articles

Citing articles: 32 View citing articles

Full Terms & Conditions of access and use can be found at
https://www.tandfonline.com/action/journalInformation?journalCode=uast20

Drag on Nonspherical Objects

David Leith
Department of Environmental Sciences and Engineering, University of North Carolina, Chapel Hill, NC 27514

Stokes's law describes drag force on a sphere in creeping flow. This law can be extended to a nonspherical object by allocating the interaction of the fluid with the object into its interaction with two analogous spheres, one with the same projected area and one with the same surface area as the object. This approach was used to characterize dynamic shape factor for objects whose shape factors are reported in the literature. Agreement between data and the equation for shape factor based on this approach was excellent for prisms: $R^2 = 0.998$. This equation and empirical equations from the literature were used to predict shape factor for a sphere, cylinders, prisms, spheroids, and double conicals whose shape factors have been reported. The equation based on the Stokes's law extension predicted shape factors better than the empirical equations, as judged by a least-squares index of performance.

INTRODUCTION

Most theory for aerosol physics derives from the assumption that particles are spheres; however, most particles are not spheres. Stokes's law, which comes from the Navier–Stokes equations for drag on an isolated sphere in creeping flow, accurately predicts drag on spheres, but does not apply to nonspherical objects.

A dynamic shape factor, K, can be defined for objects of any shape such that multiplication of the shape factor by Stokes's law drag for a sphere with the same volume as the object gives the correct drag force (Fuchs, 1964). Shape factor changes with object orientation.

$$F_D = 3\pi\mu V d_v K, \tag{1}$$

where

d_v = diameter of a sphere with the same volume as the object.

Data for shape factor are presented for objects with simple, geometric shapes, such as cubes, cylinders, rectangular prisms, spheroids, double conicals, and joined disks by Pettyjohn and Christiansen (1948), McNown and Malaika (1950), Heiss and Coull (1952), Lee et al. (1982), Johnson (1985), Sheaffer (1986), and others. Stöber and Flachsbart (1969), Davies (1979), and others present shape factors for chains of spheres. These data are useful, but are necessarily incomplete, as experiments cannot be conducted on objects with all possible shapes in all possible orientations.

Theory cannot predict shape factors, except for objects whose boundaries are easily described in relatively simple coordinate systems, because the flow field around all but the simplest shapes is impossible to define analytically. Theory can predict shape factors for spheroids and needles (Gans, 1911; Pell and Payne, 1960a), lenses and hemispheres (Payne and Pell, 1960), hollow spherical caps (Collins, 1963; Dorrepaal et al., 1978), and toroids (Pell and Payne, 1960b), and some combination of these shapes (Bowen and Masliyah, 1973); however, most particles in nature do not have these simple shapes.

Because theory is inadequate, empirical equations have been used to describe experimental results for dynamic shape factors. Most such equations were developed for axisymmetric objects such as cylinders or

Aerosol Science and Technology 6:153–161 (1987)
© 1987 Elsevier Science Publishing Co., Inc.

0278-6826/87/$3.50

spheroids, or for rectangular prisms with square cross sections. Less work has been done with rectangular prisms whose axial dimensions differ; little work has been done with objects irregular in shape.

Heiss and Coull (1952) correlate their data for cylinders and rectangular prisms with square cross sections using two empirical equations:

$$\log_{10}(K) = -0.270[(d_v/d_n) - 1] \Big/ [(\psi)^{0.5}(d_v/d_n)^{0.345}] + \log_{10}[(d_v/d_n)(\psi)^{0.5}], \quad (2)$$

for an object moving in the direction of its axis of symmetry. Here,

d_n = diameter of a sphere whose projected area is the same as the area of the object projected normal to its direction of motion, and

ψ = surface area of a sphere with the same volume as the object divided by the surface area of the object.

$$\log_{10}(K) = -0.25[\psi d_v/d_n]^{0.5} \times [(d_v/d_n) - 1] + \log_{10}[(d_v/d_n)(\psi)^{0.5}], \quad (3)$$

for an object moving normal to its axis of symmetry. No data were taken or equations given for objects with more than two independent dimensions.

Bowen and Masliyah (1973) gave an empirical equation based on the best fit to their theoretical approximations of shape factor for cylinders with flat, hemispherical, and conical ends, for merging spheres, for double-headed cones and cones with hemispherical caps, and for spheroids, all moving in the direction of their axis of symmetry.

$$K_p = 0.244 + 1.035S - 0.712S^2 + 0.441S^3, \quad (4)$$

where

$K_p = K$ based on Stokes's law drag for a perimeter-equivalent sphere,

S = surface area of the object, divided by surface area of a perimeter-equivalent sphere.

A perimeter-equivalent sphere has the same perimeter as the maximum perimeter of the object projected parallel to the direction of motion (side perimeter). For motion normal to the axis of symmetry, Clift et al. (1978) extended this idea to give

$$K = 0.392 + 0.621S - 0.040S^2. \quad (5)$$

Although Eqs. (4) and (5) were developed for objects with only two independent dimensions, Clift et al. (1978) suggested they may be useful for more complex shapes as well.

Johnson (1985) presented an empirical equation from data for orthotropic prisms.

$$K = 1/[0.197 + 0.627\psi + 0.240d_v/d_n - 0.029d_{max}/d_n], \quad (6)$$

where

d_{max} = maximum dimension of object along a principal axis.

Equation (6) appears to be the only equation in the literature specifically developed for orthotropic objects such as prisms with three unequal axes. The dimension ratios for Johnson's prisms (1985) ranged from 1 : 1 : 1 to 1 : 9.6 : 48.

Empirical equations can estimate dynamic shape factor in the absence of theory. Because the data used to develop most empirical equations are for axisymmetric or simple orthotropic objects, extrapolation is necessary to calculate the drag on objects with more complex shapes.

THEORY

The derivation of Stokes's law for drag force on a sphere shows that form drag, from pressure on the surface of the sphere, comprises one-third of the total drag. The other two-thirds, the friction drag, comes from the tangential shear stress at the sphere surface. Total drag force, F_D, is obtained by integrating the fluid pressure and the friction forces over the surface of the sphere; [see Bird et al. (1960), Hinds (1982), or Reist (1984)].

F_D = form drag + friction drag

$$= (1/3 + 2/3)3\pi\mu Vd$$

$$= 3\pi\mu Vd. \quad (7)$$

Form drag, due to integration of fluid pressure over the object surface, should be associated with the area of the object projected normal to its direction of motion. Accordingly, form drag for a nonspherical object might be expressed through the Stokes's law form drag on a sphere with the same projected area as the area of the object projected normal to its direction of motion. The diameter of this sphere is d_n.

Friction drag, due to integration of friction forces over the object surface, should be associated with the total effective surface of the object. Thus, friction drag on a nonspherical object might be expressed through the Stokes's law friction drag on a sphere with the same total surface as the object. The diameter of the sphere with equal effective surface, d_s, is

d_s = diameter of sphere whose effective surface equals that of the object.

The effective surface of the nonspherical object is the surface involved with fluid flow. As a first approximation, the effective surface might be taken as the true surface of the object. This approximation seems reasonable for objects such as prisms or spheroids. It seems less reasonable for objects with cusps or perforations, where some surface, in some orientations, will be in hydrodynamically stagnant zones.

The drag force on a nonspherical object can now be expressed through the diameters of spheres with equal projected and effective surface areas, rather than through the dimensions of the object directly.

$$F_D = 3\pi\mu V\left[(1/3)d_n + (2/3)d_s\right]$$

$$= 3\pi\mu Vd_n\left[1/3 + (2/3)(d_s/d_n)\right]$$

$$= 3\pi\mu Vd_nK_n, \quad (8)$$

where

$$K_n = \left[1/3 + (2/3)(d_s/d_n)\right]. \quad (9)$$

K_n is dynamic shape factor to be used with the Stokes's law drag equation with diameter d_n.

Equation (9) gives a theoretical expression for dynamic shape factor, and to the extent that the assumptions in its development are correct, can be used to predict the drag on objects with any shape without prior experimentation. K_nd_n can be minimized or maximized analytically for an object with given shape (prism, spheroid, etc.) to find dimension ratios that give minimum or maximum drag. For example, such an analysis predicts that a rectangular prism of fixed volume will have minimum drag, if it has relative dimensions $1:1:2\sqrt{2}$, and moves in the direction of its principal axis.

If dynamic shape factor is defined in the traditional way, using the volume equivalent diameter, d_v, Eqs. (1) and (8) show that

$$K = \left[(1/3)(d_n/d_v) + (2/3)(d_s/d_v)\right] \quad (10)$$

and

$$K_n = Kd_v/d_n. \quad (11)$$

Inclusion of d_v in Eqs. (1) and (10) is artificial because it cancels when the equations are combined. Better choices for characteristic diameter are d_n or d_s; d_n is used here.

RESULTS

Various data from the literature could be used to evaluate Eq. (9). Data from Johnson (1985) are used here because they cover a wide range of d_s/d_n, and because they include objects with three axes of symmetry rather than only two. A disadvantage of these data is that they are for prisms only.

Figure 1 is a plot of measured shape factors against d_s/d_n for the Johnson prisms. Equation (9) suggests that the plot should form a straight line with intercept of 1/3 and slope of 2/3. The data form a line that is concave upward and tangent to the theoretical line at d_s/d_n of unity. Figure 1 shows that as d_s/d_n becomes greater than unity and objects become less spherical, measured drag becomes greater than predicted. As objects become less spherical the surrounding flow field becomes less like that around a

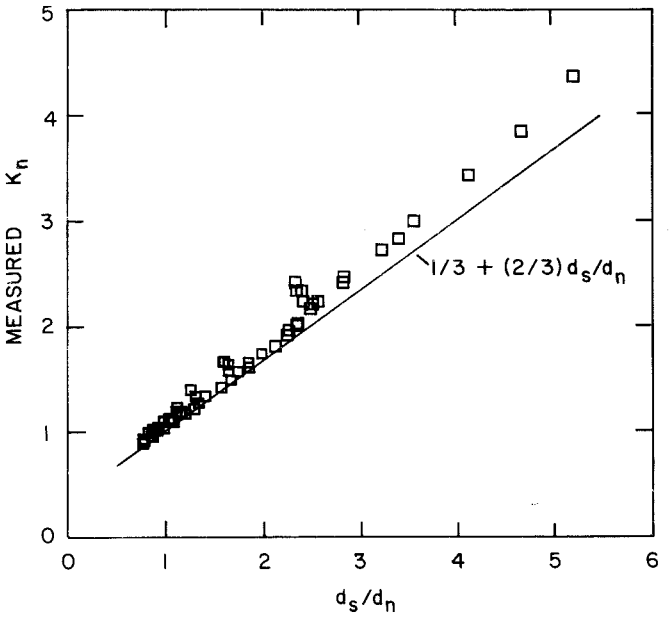


FIGURE 1. The d_n/d_s versus measured shape factor, K_n for prisms tested by Johnson (1985).

sphere, causing drag on nonspherical objects to be higher than predicted using the extension to Stokes's law.

The upward concavity of the data in Figure 1 is related to the length ratio, where

$$\text{Length ratio} = \frac{(\text{axis parallel to the direction of motion})^2}{\text{projected area normal to the direction of motion.}}$$

Sheaffer (1987) called the square of length ratio the "shape number."

Figure 1 also shows vertical "stacks" of data at d_s/d_n of about 1.7 and 2.3. Each higher point in these stacks corresponds to a prism with a larger axis ratio than that for the point below, where

Axis ratio = longest/shortest axis in the projected area normal to the direction of motion.

Least-squares regression for the Johnson data to remove the upward concavity and the vertical "stacks" by including length and axis ratios as independent variables gave

$$K_n = 0.357 + 0.684(d_s/d_n) + 0.00154(\text{length ratio}) + 0.0104(\text{axis ratio}), \quad (12)$$

for which $R^2 = 0.998$. Figure 2 is a plot of measured K_n values against predictions from Eq. (12) for the Johnson prisms. Equation (12) predicts $K_n = 1.053$ for a sphere, an error of 5.3%.

Additional data for shape factor were reported by Pettyjohn and Christiansen (1948) for a cube, by McNown and Malaika (1950) for a sphere, prisms, cylinders, and double-conicals, and by Heiss and Coull (1952) for cylinders and prisms. Fuchs (1964) reported theoretically calculated shape factors for prolate and oblate spheroids with ratios of the major to minor axis from 1.1 to 20. Sheaffer (1986) reported on prisms with dimension ratios to 1:9:92. The 91 data for shape factors that result cover a wide range of shapes and orientations.

Figures 3 to 5 show predictions for these additional data from the empirical equations of Heiss and Coull, Eqs. (2) and (3);

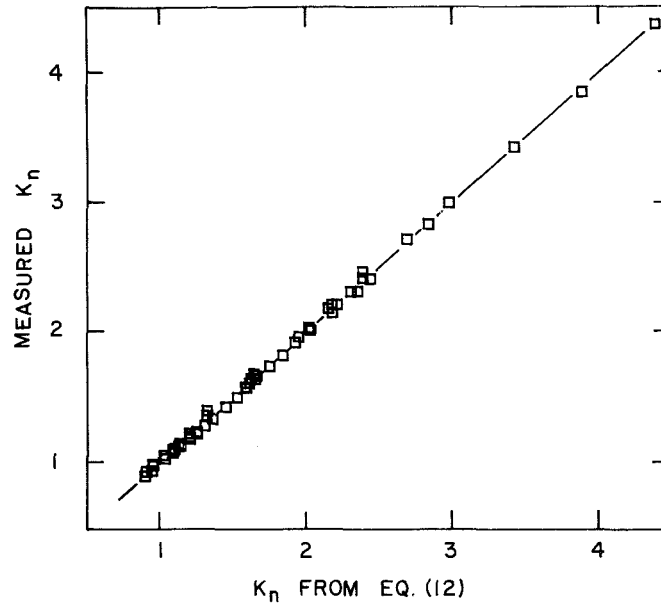


FIGURE 2. The K_n from Eq. (12) versus measured K_n for prisms tested by Johnson (1985).

Bowen–Masliyah and Clift et al., Eqs. (4) and (5); and Johnson, Eq. (6). Figure 6 shows predictions from Eq. (12). The Heiss and Coull or Bowen–Masliyah and Clift et al. equations require that the axis of symmetry be identified. For prisms with three different axial dimensions, the axis of "symmetry" was taken as that normal to the prism face closest to square.

DISCUSSION

A "least-squares performance index" used by Rudnick et al. (1986) and others can

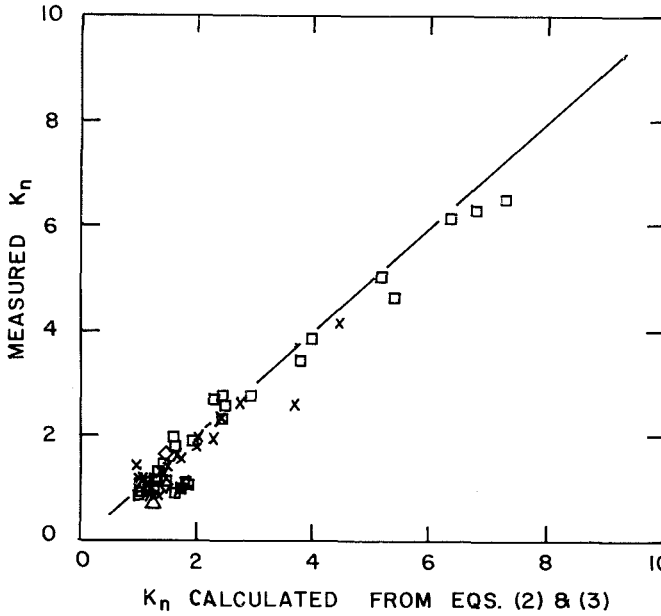


FIGURE 3. The K_n from Eqs. (2) and (3) from Heiss and Coull (1952) versus measured K_n for prisms (squares); sphere (plus); cylinders (diamonds); spheroids (crosses); and double conicals (triangles).

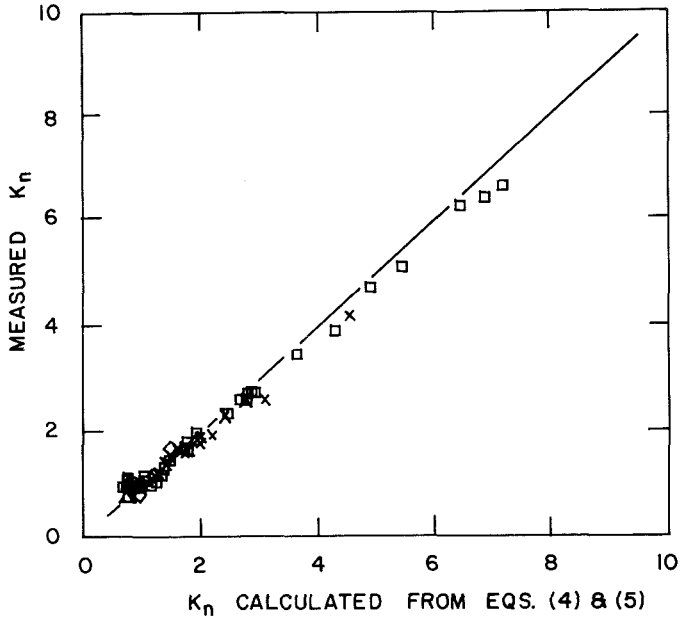


FIGURE 4. The K_n calculated from Eqs. (4) and (5) from Bowen–Masliyah (1973) and Clift et al. (1978) versus measured K_n for prisms (squares); sphere (plus); cylinders (diamonds); spheroids (crosses); and double conicals (triangles).

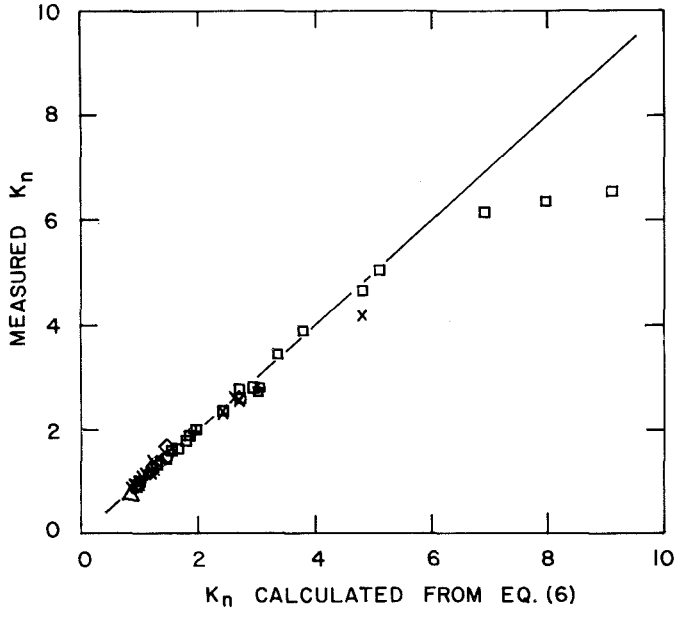


FIGURE 5. The K_n calculated from Eq. (6) from Johnson (1985) versus measured K_n for prisms (squares); sphere (plus); cylinders (diamonds); spheroids (crosses); and double conicals (triangles).

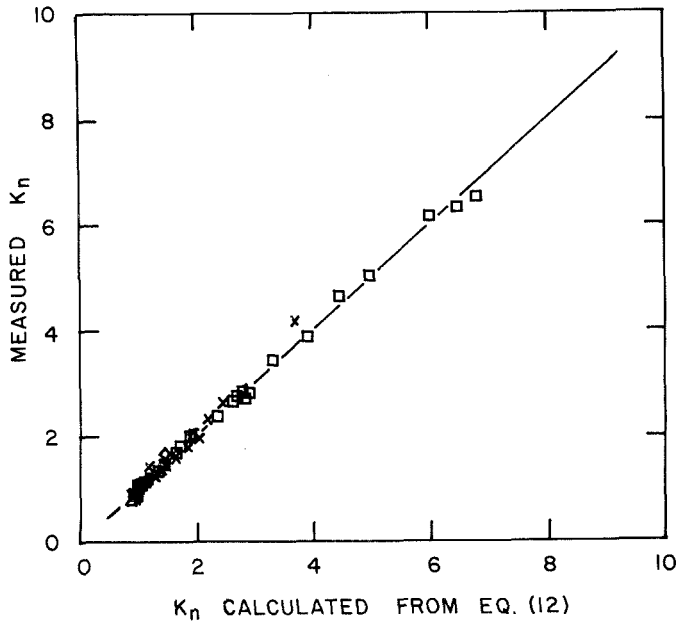


FIGURE 6. The K_n calculated from Eq. (12) versus measured K_n for prisms (squares); sphere (plus); cylinders (diamonds); spheroids (crosses); and double conicals (triangles).

evaluate agreement between predictions and data. The index, I, is found for each model from

$$I = \left[\Sigma\left(K_{n,\,\text{measured}} - K_{n,\,\text{predicted}}\right)^2\right]/n$$
$$= [\Sigma\Delta^2]/n \qquad (13)$$

where n is the number of data and I is the quantity minimized when a regression line is fit to data by the least-squares method.

The performance index has two components. The first, $\bar{\Delta}$, is the average difference between data and predicted values.

$$\bar{\Delta} = \left[\Sigma\left(K_{n,\,\text{measured}} - K_{n,\,\text{calculated}}\right)\right]/n. \qquad (14)$$

The second component is the variance of Δ, by definition

$$\sigma_\Delta^2 = \frac{\Sigma(\Delta - \bar{\Delta})^2}{n-1} = \frac{\Sigma\Delta^2}{n-1} - \frac{(\Sigma\Delta)^2}{n(n-1)}. \qquad (15)$$

If n is large,

$$I \doteq (\bar{\Delta})^2 + \sigma_\Delta^2. \qquad (16)$$

Therefore, the two components of I are $\bar{\Delta}$, a measure of the average difference between measured and predicted K_n values, and σ_Δ^2, a measure of the scatter about the $K_{n,\,\text{measured}} = K_{n,\,\text{predicted}}$ line. For a model that predicts data well, both $\bar{\Delta}$ and σ_Δ^2 will be small, resulting in small I. For the data and models examined here, Table 1 presents values of $\bar{\Delta}$, σ_Δ^2, and I.

Figure 3, the plot of predicted versus measured K_n values for the Heiss and Coull equations, shows that these equations predicted K_n fairly well. The equations overestimated K_n by 0.12 on the average. The variance was relatively high, as can be seen by the considerable scatter of the data in Figure 2. The resultant performance index was relatively high.

Figure 4, a comparable plot for the Bowen–Masliyah, and Clift et al. equations, shows that they predicted K_n well, but overestimated measured K_n by $+0.021$ on average. The overestimation apparently increased as the objects became more extreme in shape. The variance for these equations was somewhat high and is responsible for the larger part of the performance index.

TABLE 1. Performance Indexes for Shape Factor Equations

	Heiss and Coull	Bowen–Masliyah and Clift et al.	Johnson	Eq. (12)
Mean difference, $\bar{\Delta}$	0.119	0.021	0.059	−0.007
Variance, σ_Δ^2	0.088	0.037	0.117	0.010
Index, I	0.101	0.037	0.119	0.010
t	4.11	3.40	1.41	—

Note: t-test for comparison between Eq. (12) and other models.

Figure 5, for the Johnson equation, shows that this relationship predicted K_n very well except for objects with extreme shapes, beyond the K_n values for which this empirical equation was developed. On average, the Johnson equation overestimated K_n by 0.059. The high variance, 0.117, was due to the three or four objects with extreme shapes and high K_n values.

Figure 6, for Eq. (12), shows that this equation predicted K_n well for all data. On average, the equation underestimated K_n values slightly, by 0.007. The variance in these values was small at 0.010, and the performance index for Eq. (12) was the lowest of all models tested.

A paired t-test can determine whether the I values for model pairs are significantly different. Results of comparisons between all models and Eq. (12) are also shown in Table 1. These tests show that Eq. (12) had a significantly better (lower) performance index than the Heiss and Coull or Bowen–Masliyah and Clift et al. models ($p < 0.01$). The performance index for Eq. (12) was also better (lower) than that for the Johnson equation, but not significantly better at the 5% confidence level. Comparison of Figures 5 and 6 shows that both equations predicted the data well for objects with shapes that are not extreme. Equation (12) may have predicted K_n better for objects with extreme shapes; however, insufficient data for objects with extreme shapes were available to be sure this trend was significant.

The theory by itself, Eq. (9), predicted the increase in K_n with increasing d_s/d_n shown in experiments; see Figure 1. Two additional terms with empirically determined coefficients were necessary to obtain the excellent agreement between K_n predictions and data given by Eq. (12). The advantage of calibrated theory over complete empiricism is that theory points out parameters that should affect drag for nonspherical objects, and so suggests areas where further research is likely to be fruitful. For example, theory refinement may be possible by further exploration of the effective surface concept. Research in this area is under way.

REFERENCES

Bird, R. B., Stewart, W. E., and Lightfoot, E. N. (1960). *Transport Phenomena*. Wiley, New York, p. 132.

Bowen, B. D., and Masliyah, J. H. (1973). *Can. J. Chem. Eng.* 51:8–15.

Brenner, H. (1962). *Journal of Fluid Mechanics* 12:35–48.

Clift, R., Grace, J. R., and Weber, M. E. (1978). *Bubbles, Drops, and Particles*. Academic Press, New York, p. 85.

Collins, W. D. (1963) *Mathematika* 10:72–78.

Davies, C. N. (1979). *J. Aerosol Sci.* 10:477–513.

Dorrepaal, J. M., O'Neill, M. E., and Ranger, K. B. (1978). *J. Fluid Mech.*75:273–286.

Fuchs, N. A. (1964). *The Mechanics of Aerosols*. Pergamon, Oxford, U.K., p. 39.

Gans, R. (1911). *Sitzungsber. Math-Physik Klasse Akad. Wissen. Munchen* 41:198–203.

Heiss, J. F., and Coull, J. (1952). *Chem. Eng. Prog.* 48:133–140.

Hinds, W. (1982). *Aerosol Technology*. Wiley Interscience, New York, pp. 62–65.

Johnson, D. L. (1985). *Drag Force on Orthotropic Aerosol Particles*. Ph.D. thesis, University of North Carolina at Chapel Hill.

Lee, P. S., Niida, T., and Shaw, D. T. (1982). *Aerosol Sci. Technol.* 1:259–270.

McNown, J. S., and Malaika, J. (1950). *Trans. Am. Geophys. Union* 31:74–82.

Payne, L. E., and Pell, W. H. (1960). *J. Fluid Mech.* 7:529–549.

Pell, W. H., and Payne, L. E. (1960–1961a). *Q. Appl. Math.* 18:257–262.

Pell, W. H., and Payne, L. E. (1960b). *Mathematika* 7:78–92.

Pettyjohn, E. S., and Christiansen, E. B. (1948). *Chem. Eng. Prog.* 44:157–172.

Reist, P. C. (1984). *Introduction to Aerosol Science.* MacMillan, New York, pp. 275–277.

Rudnick, S. N., Koehler, J., Martin, K. P., Leith, D., and Cooper, D. W. (1986). *Environ. Sci. Technol.* 20:237–242.

Sheaffer, A. (1987). *J. Aerosol Sci.*, in press.

Stöber, W., and Flachsbart, H. (1969). *Environ. Sci. Technol.*, 3:1280–1296.

Received 11 November 1985; accepted 3 April 1986